JBC RESEARCH ARTICLE

N-terminal acetylation and arginylation of actin determines the architecture and assembly rate of linear and branched actin networks

Received for publication, May 11, 2022, and in revised form, September 16, 2022 Published, Papers in Press, September 22, 2022,
https://doi.org/10.1016/j.jbc.2022.102518

Samantha M. Chin[1], Tomoyuki Hatano[2], Lavanya Sivashanmugam[2], Andrejus Suchenko[2], Anna S. Kashina[3], Mohan K. Balasubramanian[2], and Silvia Jansen[1,*]

From the [1]Department of Cell Biology and Physiology, Washington University in St Louis, Saint Louis, Missouri, USA; [2]Centre for Mechanochemical Cell Biology and Division of Biomedical Sciences, Warwick Medical School, University of Warwick, Coventry, UK; [3]Department of Biomedical Sciences, School of Veterinary Medicine, University of Pennsylvania, Philadelphia, Pennsylvania, USA

Edited by Enrique De La Cruz

The great diversity in actin network architectures and dynamics is exploited by cells to drive fundamental biological processes, including cell migration, endocytosis, and cell division. While it is known that this versatility is the result of the many actin-remodeling activities of actin-binding proteins, such as Arp2/3 and cofilin, recent work also implicates posttranslational acetylation or arginylation of the actin N terminus itself as an equally important regulatory mechanism. However, the molecular mechanisms by which acetylation and arginylation alter the properties of actin are not well understood. Here, we directly compare how processing and modification of the N terminus of actin affects its intrinsic polymerization dynamics and its remodeling by actin-binding proteins that are essential for cell migration. We find that in comparison to acetylated actin, arginylated actin reduces intrinsic as well as formin-mediated elongation and Arp2/3-mediated nucleation. By contrast, there are no significant differences in cofilin-mediated severing. Taken together, these results suggest that cells can employ these differently modified actins to regulate actin dynamics. In addition, unprocessed actin with an N-terminal methionine residue shows very different effects on formin-mediated elongation, Arp2/3-mediated nucleation, and severing by cofilin. Altogether, this study shows that the nature of the N terminus of actin can promote distinct actin network dynamics, which can be differentially used by cells to locally finetune actin dynamics at distinct cellular locations, such as at the leading edge.

Actin cytoskeleton dynamics are the driving force for a myriad of essential cellular functions, including cell migration, cytokinesis, intracellular transport, and contractility (1–3). The functional diversity of actin stems in part from its intrinsic ability to rapidly and reversibly transition between monomeric and filamentous forms and is further expanded through tight spatiotemporal control by hundreds of actin-binding proteins with specific actin-remodeling activities (4). In addition, it is becoming increasingly clear that direct modification of actin molecules, for example by phosphorylation, acetylation, arginylation, methylation, or oxidation, can have profound effects on actin network dynamics (5–10).

Modification of actin can occur on many of its exposed residues, including its very N terminus (9). The latter is of special interest, as it is the most divergent region in the well-conserved actin molecule, and its modification could be expected to generate unique ways to regulate actin cytoskeleton dynamics. In line with this, posttranslational modification of the N terminus of the abundant cytoplasmic β-actin by mutually exclusive acetylation or arginylation is emerging as a first-line mechanism to regulate cell migration (11–13). Like its cytoplasmic partner γ-actin, the N-terminal initiator Met of β-actin is removed cotranslationally, thereby exposing the second residue (Asp2 in β-actin, Glut2 in γ-actin) for further modification by acetylation (14). Although this extensive processing of the N terminus of actin was characterized ∼30 years ago, it was not until recently that it was shown that acetylation of the exposed acidic residue is mediated by a dedicated N-acetyltransferase, NatH/NAA80, which specifically diverged to only target the acidic N terminus of all six human actins (15, 16). Surprisingly, NAA80 KO cells are hypermotile and show significant increases in the number of filopodia and total F-actin content, whereas *in vitro* assays show that nonacetylated β/γ-actin displays slower filament elongation than acetylated β/γ-actin, even in the presence of formins (11). This leaves open the question of how acetylation of actin mechanistically contributes to curbing cell migration.

The N terminus of the cytoplasmic actins can be further trimmed down to the second acidic residue, which then can be arginylated by the nonspecific arginyltransferase Ate1 (7, 17). Interestingly, arginylation in combination with slower translation leads to immediate proteasomal degradation of γ-actin (18). As a result, only arginylated β-actin (hereafter referred to as R-actin) is detected in cells, where it has been shown to specifically relocate to the leading edge upon induction of cell migration (12). Although less than 1% of the total β-actin population is estimated to be arginylated (19), making it highly challenging to detect in whole cell lysates (20); it is possible

* For correspondence: Silvia Jansen, silvia.jansen@wustl.edu.

that local concentrations at the leading edge during active cell migration are much higher and thus exert significant effects on local actin cytoskeleton dynamics. However, both actin as well as various actin-binding proteins can be modified by Ate1, making it difficult to identify what role and which actin-remodeling activities are directly influenced by arginylation of β-actin (R-actin) (17). Also, NAA80 KO cells show a 7-fold increase in R-actin (17, 20), which supports the hypothesis that acetylation and arginylation of β-actin are mutually exclusive and that the enhanced motility of NAA80 KO cells might at least in part be due to the increased presence of the more positively charged R-actin. This strongly suggests that acetylated (Ac-actin) and R-actin have different intrinsic dynamics and/or interact differently with key actin-regulatory proteins that control cell migration; however, the underlying molecular mechanisms remain unclear to date.

Here, we have used pick-ya-actin, a recently established method to produce pure populations of specifically modified human β-actin in *Pichia pastoris*, to perform the first direct comparison between acetylated and arginylated mammalian β-actin (21, 22). To get a better understanding of the contribution of N-terminal modification of β-actin to actin filament dynamics, we also included pure populations of unprocessed actin with an N-terminal methionine (M-actin). Bulk pyrene fluorescence and total internal refection fluorescence microscopy (TIRFM) analysis elucidated that these actins have distinct intrinsic polymerization properties and interact differently with key actin-binding proteins, including profilin, mDia1, Arp2/3, and cofilin. Altogether, this study shows for the first time that proper processing and different N-terminal modifications of actin can alter actin network dynamics and may thusly provide an extra layer of cytoskeletal regulation in cells.

Results and discussion

Acetylation of actin markedly facilitates actin filament nucleation

The N terminus of β-actin is cotranslationally processed to prepare it for further modification by either acetylation on Asp2 or arginylation on Asp3; however, it remains unclear how this extensive processing and subsequent modification affect the intrinsic self-assembly dynamics of β-actin. To investigate this, Ac-β-actin (Ac-actin), R-β-actin (R-actin), and unprocessed β-actin (M-actin) were recombinantly produced using the recently developed pick-ya-actin system (21, 22). Mass spec analysis confirmed that the purified actins consisted of a pure population of actin monomers that underwent the specified modification or different processing of their N terminus (21, 22). Next, we compared the polymerization of these different actins using bulk fluorescence assays and TIRFM. Both methods show that Ac-actin polymerizes faster than any of the other tested actins, whereas R-actin was observed to consistently assemble the slowest of all actins (Fig. 1, *B–F* and Movie S1). TIRFM further enabled us to directly visualize and accurately quantify effects on actin filament nucleation *versus* actin filament elongation. This analysis showed that spontaneous actin filament nucleation was about 5-fold higher for Ac-actin compared to any of the other actins (Figs. 1, *D* and *E* and S1). By contrast, individual actin filaments assembled from each actin were observed to elongate at similar rates (Fig. 1*F*). Altogether, these independent methods demonstrate that there are clear differences in the intrinsic polymerization and spontaneous nucleation of R-actin and Ac-actin, suggesting that specific modification of the actin N terminus can alter actin filament polymerization.

Formin-mediated polymerization is reduced by N-terminal arginylation of actin

In cells, actin monomers are sequestered by profilin-1 (hereafter referred to as PFN), which curbs spontaneous nucleation and regulates actin filament assembly (23–25). Given the differences observed in spontaneous nucleation of Ac-actin and R-actin, we next examined whether modification of the N terminus of actin changes its binding and sequestration by PFN. To this end, actin filaments were polymerized in the presence of increasing concentrations of PFN, pelleted by centrifugation, and analyzed by densitometry. The fraction of filaments in the pellet was used to determine binding of the differently modified actin monomers by PFN (Figs. 2*A* and S2). This analysis showed that PFN associates similarly with actins with different N-terminal modifications. This is in agreement with a recent structure of monomeric actin bound to PFN and Ac-CoA-NAA80 (16), which uniquely enabled to resolve the N terminus of actin. This structure shows that the N terminus of actin is located distally from the PFN binding site and thus should not be affected by N-terminal modification (16). Importantly, our data further suggest that in cells, assembly of PFN-bound Ac-actin and R-actin is regulated by additional actin-nucleating proteins.

Having established that PFN interacts similarly with Ac-actin and R-actin, we next analyzed whether N-terminal modification of actin affects formin-mediated assembly. Formins are homodimers that stimulate filament nucleation and elongation, preferentially from PFN-bound actin monomers, using their formin homology domains (FH1 and FH2) (26). The FH2 domain dimerizes to nucleate actin filaments and remains processively associated with the barbed end of a growing filament, whereas the unstructured FH1 domain binds and positions the PFN-actin complex for addition to the growing filament end.

Given that the N terminus is modeled to protrude from the filament (8, 16), this suggests that the more positively charged N terminus resulting from arginylation might change the overall charge of the actin filament, thus potentially altering the interaction of formins, such as mDia1. Indeed, bulk pyrene fluorescence assays showed that filament polymerization by mDia1 was severely decreased for R-actin (Fig. 2, *B* and *C*). TIRFM further demonstrated that nucleation of Ac-actin by PFN and mDia1 was similar to nucleation of R-actin and about two-fold decreased compared to the nucleation of M-actin (Fig. 2*E*). Analysis of individual filaments showed slower mDia1-mediated elongation for both Ac-actin and R-actin

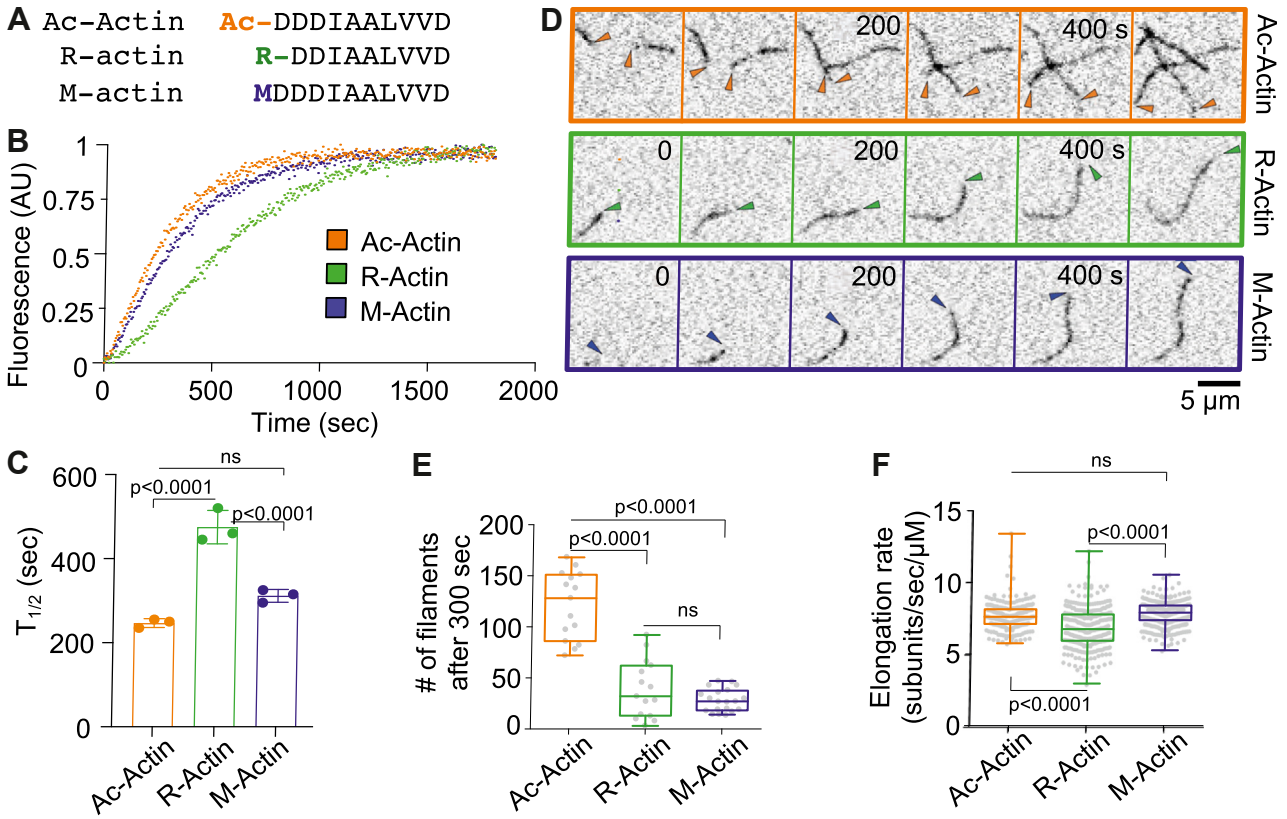

Figure 1. Intrinsic actin filament assembly of differentially modified actins. *A*, overview of the different β-actins used in this study. *B*, polymerization of 4 μM of actin monomers (+10% pyrene-labeled RMA) carrying the indicated N-terminal modification. Data shown are a representative example of three independent experiments. *C*, assembly curves as shown in (*B*) were used to determine the time to half-maximal polymerization ($T_{1/2}$). *D*, montages of representative TIRF microscopy movies showing the intrinsic self-assembly of 1 μM of the indicated actins (+15% Alexa488 RMA). *E* and *F*, distribution of spontaneous actin filament nucleation (*E*) and filament elongation rate (*F*) of the differently modified actins of three independent experiments. Corresponding box and whisker plots, indicating minimum, maximum, and median, are shown as overlays. Statistical significance was analyzed using one-way ANOVA with a Tukey post-hoc test (N = 3).

compared to M-actin filaments (Fig. 2, *D* and *F* and Movie S2). Polymerization of R-actin by mDia1 was only slightly slower than mDia1 elongation of Ac-actin (14.0 ± 0.3 subunits/sec/μM *versus* 19.3 ± 0.5 subunits/sec/μM). However, our bulk pyrene assays suggest that at higher actin concentrations, such as found in cells, this small difference in elongation rate may result in substantially different total actin mass. Altogether, our pyrene fluorescence and TIRFM data indicate that formin-mediated elongation is sensitive to the nature of the actin N terminus.

Arp2/3-mediated nucleation is sensitive to the nature of the N terminus of actin

R-actin shows a distinct lamellipodial localization in migrating cells (12), suggesting that it is not only used for formin-mediated elongation but also participates in the formation of the extensive branched networks underneath the protruding cell membrane. In line with this, the branched actin network at the leading edge of Ate1 KO cells is severely disorganized, although it remains unclear whether this stems from arginylation of β-actin or the Arp2/3 complex, as both were identified as Ate1 targets (17). Our approach with isoform-pure and singly modified actin uniquely enables us to investigate the direct effects of arginylation of β-actin on Arp2/3-mediated actin filament nucleation and branching and get a better insight into the role of arginylation on branched actin network dynamics. Also, it is unknown whether R-actin accumulation at the leading edge can stimulate cell polarization, protrusion, or retraction of the lamella. To this end, we tested the effect of arginylation of the N terminus of actin on Arp2/3 networks using the well-studied and well-characterized GST-VCA domain of NWASP over the less used and understood VCA domains of other nucleation promoting factors.

Bulk pyrene fluorescence assays showed that Arp2/3-mediated nucleation of R-actin was severely reduced (Fig. 3, *A* and *B*). In addition, M-actin slightly increased Arp2/3-mediated nucleation compared to Ac-actin. Similar trends were observed when analyzing these actins in TIRFM (Fig. 3, *C* and *D*). Branch rate analysis showed significantly decreased formation of branches from the sides of filaments that were polymerized from R-actin, whereas M-actin slightly increased Arp2/3 branching (Fig. 3, *C* and *D* and Movie S3). Thus, like formin-mediated elongation, Arp2/3-mediated nucleation is hampered by arginylation (R-actin *versus* Ac-actin and M-actin), suggesting that the charge of the N terminus can alter interaction of actin-binding proteins with actin filaments. However, in case of Arp2/3-mediated nucleation, it is unclear

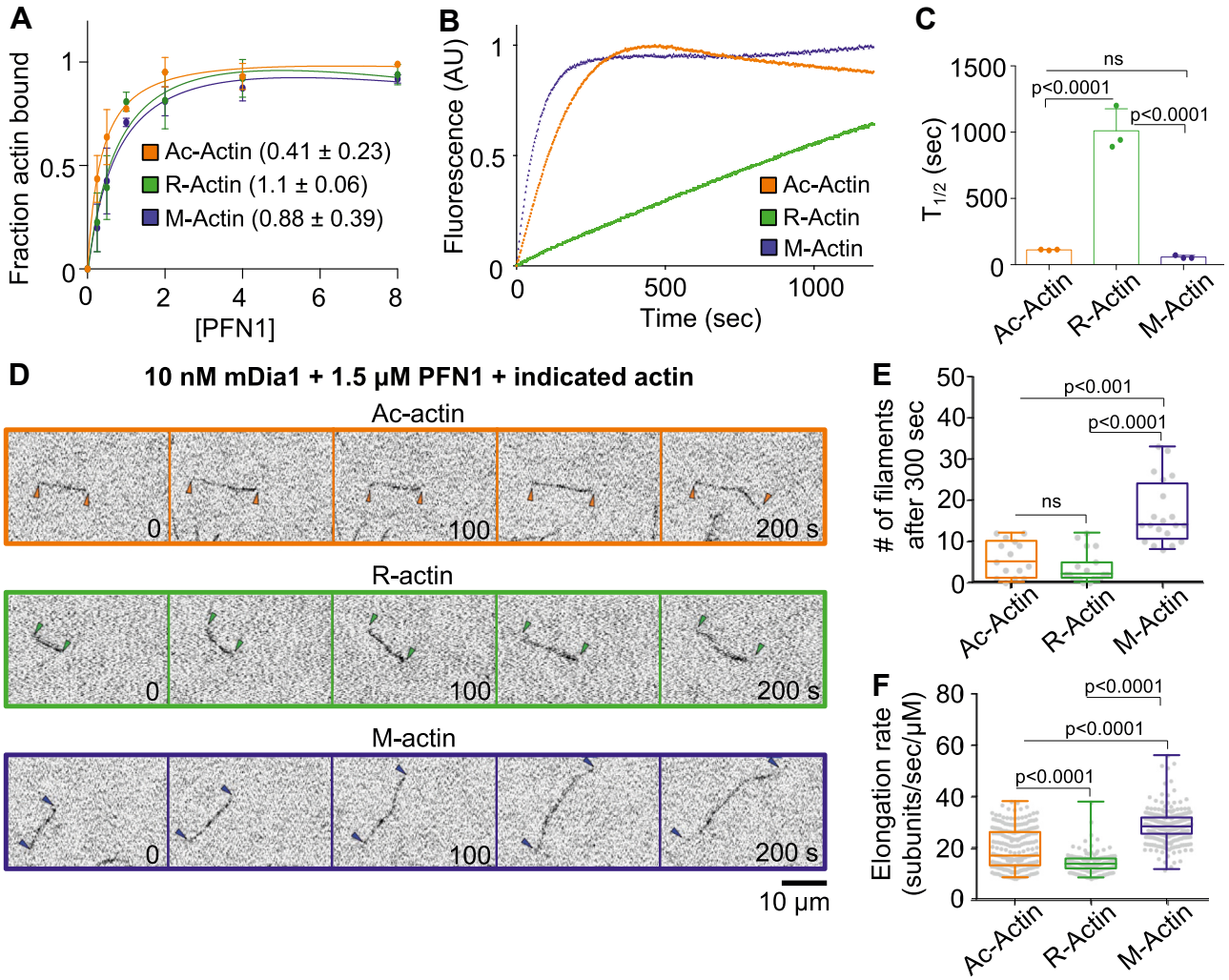

Figure 2. N-terminal modification of actin affects formin-mediated filament assembly. *A*, fraction of actin bound to PFN calculated from inhibition of actin polymerization induced by increasing concentrations of PFN was measured by Coomassie staining and densitometry. Curves were fit using nonlinear regression of data obtained from three independent experiments. *B*, polymerization of 2 µM of the indicated actin (+5% pyrene-labeled RMA) in the presence of 1 µM PFN and 20 nM mDia1 (FH1-FH2). Curves shown are from one representative example of three independent experiments. *C*, assembly curves as shown in (*B*) were used to determine the time to half-maximal polymerization ($T_{1/2}$). *D*, montages of representative TIRF microscopy movies of 1 µM of the indicated actins (+15% Alexa488 RMA) with 10 nM mDia1 and 1.5 µM PFN. *Arrowheads* indicate the growing filament. Distribution of mDia1-mediated actin filament nucleation (*E*) and elongation (*F*) of actins with different N-terminal modifications derived from movies as shown in (*D*). Data were obtained from three independent experiments. Corresponding box and whisker plots, indicating minimum, maximum, and median, are shown as overlays. All *p*-values were obtained by comparing the indicated actins using one-way ANOVA with a Tukey post-hoc test (N = 3). PFN, profilin-1.

whether this is due to decreased binding of Arp2/3 to arginylated mother filaments or decreased binding of arginylated actin monomers to NWASP.

N-terminal modification has mild effects on cofilin-mediated severing

Our observations show that both formin-mediated filament assembly and Arp2/3-mediated filament nucleation are sensitive to N-terminal modification of actin. However, both Arp2/3 as well as formins are bulky molecules that can be more easily affected by changes in the overall charge and surface of actin filaments. Thus, we next tested whether N-terminal modification of actin also changes the interaction of a small actin-binding molecule. For this purpose, we chose the F-actin disassembly factor, cofilin. We directly compared cofilin-mediated severing of Ac-actin and R-actin filaments using TIRFM. Our results show a small reduction in the cumulative severing rate of R-actin compared to Ac-actin; however, this slight decrease did not significantly change the time to half-maximal severing (Fig. 4, *B* and *C* and Movie S4). Surprisingly, fragmentation of unprocessed M-actin was enhanced in comparison to Ac-actin and R-actin. Taken together, our data show that interaction of cofilin with physiologically relevant acetylated and arginylated actin filaments is similar *in vitro*. Combined with our previous results on actin assembly by formins and Arp2/3, this suggests that under cellular conditions, modification of the actin N terminus more likely affects actin network assembly than disassembly. However, our observations for M-actin do leave the possibility that a yet unidentified N-terminal modification may make actin filaments more prone to cofilin-mediated severing. As such, it would be of interest to know whether the enhanced severing seen by M-

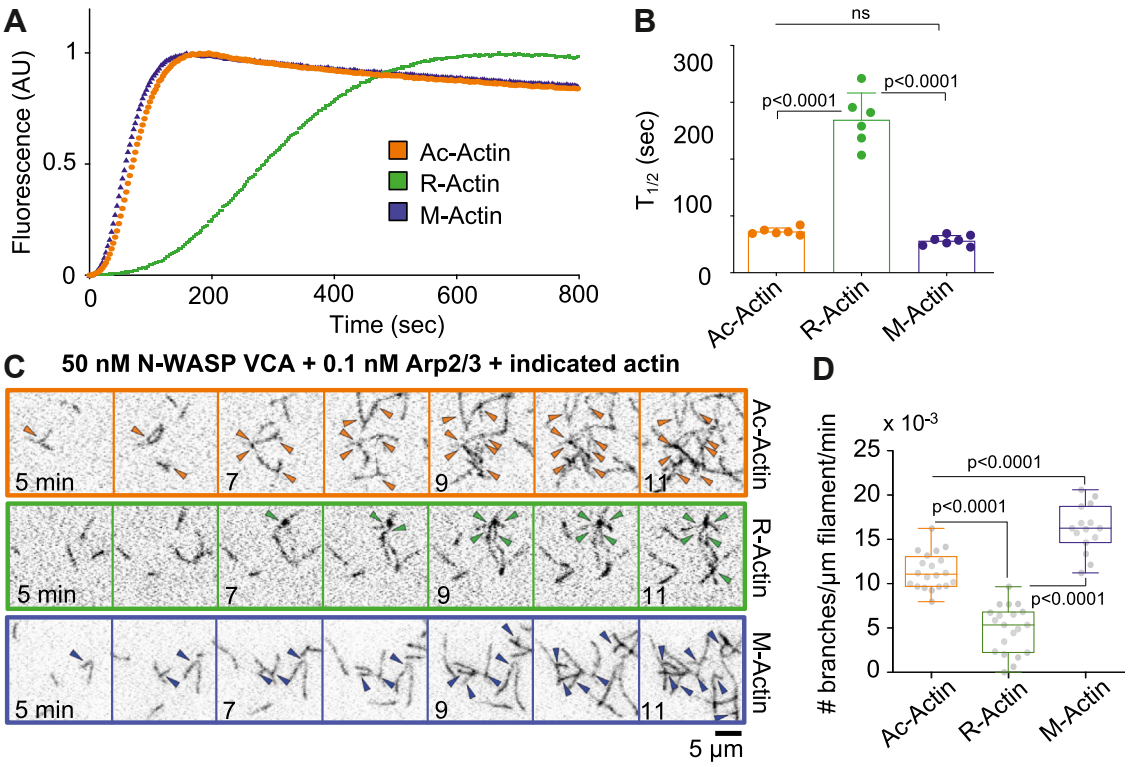

Figure 3. Arp2/3-mediated branching using differentially modified actins. *A*, polymerization of 2 μM of the indicated actin (+5% pyrene-labeled RMA) in the presence of 25 nM GST-VCA and 10 nM Arp2/3. A representative example of three independent experiments is shown. *B*, assembly curves as shown in (*A*) were used to determine the time to half-maximal polymerization ($T_{1/2}$). *C*, montages of representative TIRF microscopy movies of 1 μM of the indicated actins (+15% Alexa488 RMA) with 50 nM GST-VCA and 0.1 nM Arp2/3. *Arrowheads* indicate newly formed actin branches. *D*, distribution of branching rates of the different actins from at least three independent experiments. Corresponding box and whisker plots, indicating minimum, maximum, and median, are shown as overlays. Statistical significance was analyzed using one-way ANOVA with a Tukey post-hoc test (N = 3).

actin is due to altered cooperative binding of cofilin to the M-actin filament being more prone to the conformational changes induces by cofilin, remains an open question.

Equimolar concentrations of R-actin can affect actin network assembly by Ac-actin

Our results show that branched and formin-mediated actin networks are assembled differently from pure populations of Ac-actin, and R-actin. However, in cells, both Ac-actin and R-actin localize to the leading edge, which raises the question how actin network assembly is regulated in the presence of both modified actins. To investigate this, we measured formin-mediated assembly and Arp2/3-mediated nucleation of Ac-actin mixed with an increasing percentage (0–60%) of R-actin in bulk pyrene assays. In line with our previous observations, assembly using 100% R-actin monomers was severely reduced compared to assembly from 100% Ac-actin monomers (Fig. 5*A*). Spiking in 10% R-actin into Ac-actin slightly reduced actin filament assembly compared to 100% Ac-actin, and this effect became more pronounced with increasing percentages of R-actin (Fig. 5*A*), suggesting that changes in the ratio of R-actin to Ac-actin can alter the rate of actin polymerization.

A recent study showed that R-actin can locally accumulate to ∼25% of actin at the leading edge (19). Thus, we analyzed specifically whether a 1:3 ratio of R-actin to Ac-actin (25% R-actin with 75% Ac-actin) can change actin polymerization in bulk pyrene fluorescence assays. Analysis of the half-times showed that the presence of 25% R-actin did not significantly alter polymerization compared to actin polymerization by Ac-actin only (Fig. 5, *B* and *C*). By contrast, slightly different polymerization of Ac-actin was observed at a 1:1 ratio of R-actin to Ac-actin (Fig. 5, *B* and *C*). Altogether, these data demonstrate that for cellular actin network polymerization to be affected by R-actin, the local concentration of R-actin needs to increase to or above the concentration of Ac-actin to influence mDia1-mediated elongation and Arp2/3-mediated nucleation.

Conclusions

It has been known for many years that actin monomers and filaments can undergo a multitude of modifications; however, the functional impact of many of these modifications remains elusive. Here, we used a recently established system to generate specifically modified actins in Pichia and show that N-terminal modification can have a profound effect on actin filament assembly. Specifically, we focus on directly comparing the effect of arginylation and acetylation of the N terminus of β-actin on actin-binding proteins that shape the actin networks at the leading edge. In addition, we assessed the effects

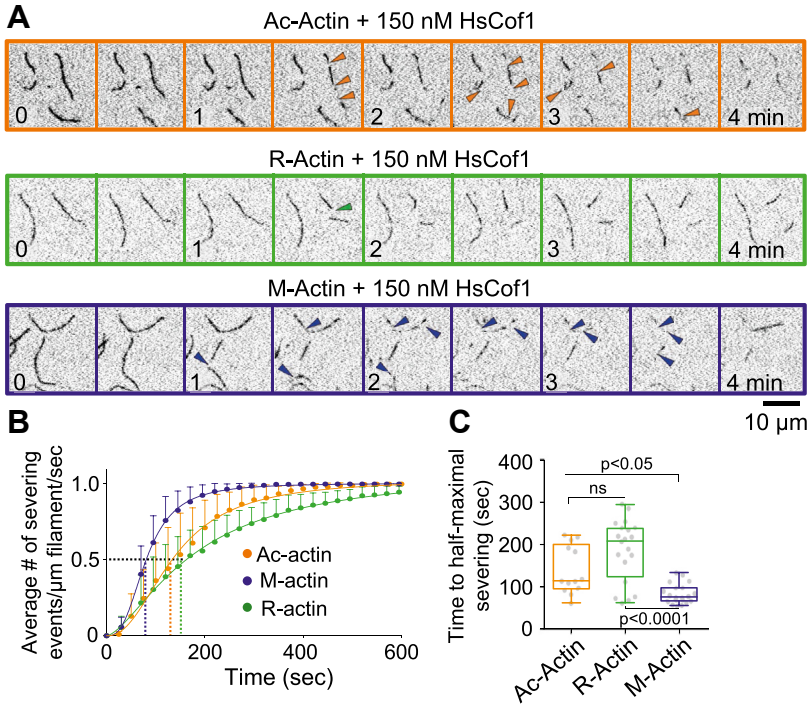

Figure 4. Cofilin-mediated severing of differentially modified actins. *A*, montages of representative TIRF microscopy movies of 1 µM of the indicated actins (+15% Alexa488 RMA) with 150 nM cofilin. *Arrowheads* indicate severing events. *B*, cumulative severing of the indicated modified actins shown as the average ± SD of three independent experiments. *C*, distribution of time to half-maximal severing calculated from the cumulative severing curves shown in (*B*). Corresponding box and whisker plots are shown as overlays. Statistical significance was tested by comparing the different actins using one-way ANOVA with a Tukey post-hoc test (N = 3).

of proper processing of the actin N terminus using a non-physiological M-actin.

Our results, summarized in Table 1, show that spontaneous nucleation of Ac-actin is much higher than that of R-actin *in vitro* (Fig. 1). This is in agreement with an earlier study, which showed that actin isolated from Ate1 knockout cells nucleates faster than actin isolated from WT cells in bulk pyrene fluorescence assays (27). In addition, recent work by Drazic *et al.* (11) also demonstrated that Ac-actin has a higher elongation rate than nonacetylated actin. Altogether, these three studies emphasize that N-terminal modification of actin monomers is important for actin filament dynamics *in vitro* and thus may affect remodeling of actin networks by actin-binding proteins in cells.

In line with this, R-actin showed severely reduced elongation by mDia1 as well as decreased nucleation and branching by Arp2/3 compared to Ac-actin (Figs. 2, *B–F*and 3). This first seemed at odds with the cellular phenotype observed for NAA80 KO cells, which show a marked increase in F-actin and in the number of filopodia (11). However, despite the fact that these cells produce 7-fold more R-actin, this only increases the percentage of R-actin from 0.8 to 5.3% of the total actin population (19). As a result, these cells mostly produce non-acetylated actin (DDD-actin), which we did not include in this study. As our work further shows that there is no significant difference in cofilin-mediated severing between Ac-actin and R-actin (Fig. 4), this suggests that the increase in filopodia observed in the absence of N-acetylation of actin is more likely due to altered actin assembly than disassembly kinetics.

Based on our results, Ac-actin and R-actin can co-assemble into linear and branched actin networks at the leading edge; however, an equimolar to higher concentration of R-actin to Ac-actin is required to significantly change actin polymerization (Fig. 5, *B* and *C*). Given that R-actin constitutes less than 1% of the total β-actin population and only increases to 5.3% in NAA80 KO cells, this suggests that R-actin needs to be locally increased to exert effects on actin dynamics. In line with this, lamellar R-actin has been observed to accumulate at the leading edge at distinct spots; however, the percentage of R-actin at these hot spots was estimated to be no higher than ∼25% (19). This raises the question whether the effects of N-terminal arginylation in cells are perhaps compounded by any of the many other intramolecular modifications reported for actin (9). In line with this, a recent study showed that actin filament elongation by the formin, INF2, is inhibited by a complex of Srv2/CAP and lysine-acetylated actin (5, 28). It would be interesting to test whether acetylation of these lysine residues work synergistically with N-terminal arginylation of actin in blocking actin assembly by mDia1, INF2, or any of the other formins. Other prevalent modifications include methylation of His73 of actin by the methyltransferase SETD3, which has been shown to slightly accelerate actin assembly and oxidation of Met40 of actin by MICAL, which induces actin depolymerization (6, 10). However, it remains an open question how each of these modifications work in combination with N-terminal acetylation and arginylation of actin to regulate actin dynamics *in vitro* and in cells.

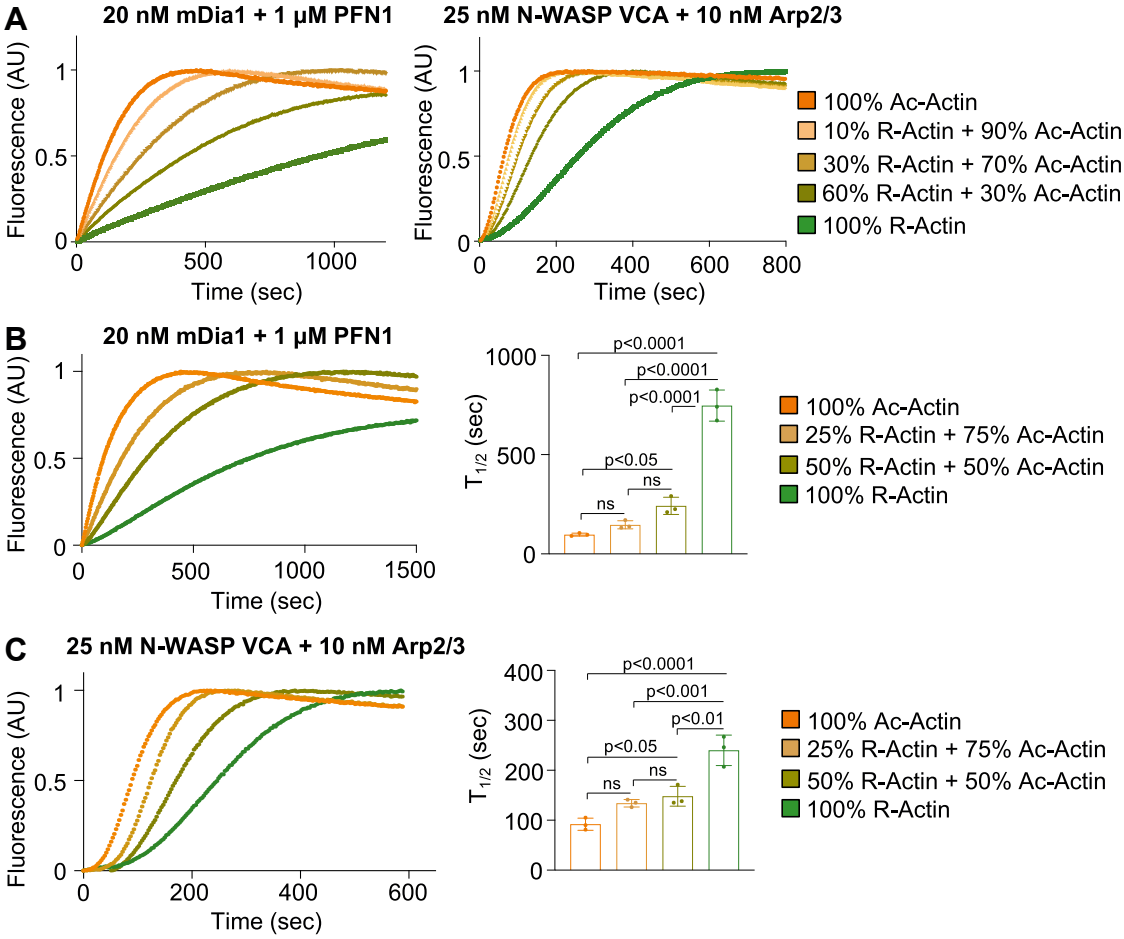

Figure 5. Combined effects of Ac-actin and R-actin on actin assembly. *A*, polymerization of 2 μM (+5% pyrene-labeled RMA) of actin composed of the indicated ratios of Ac-actin and R-actin in the presence of PFN and mDia1 (left graph) or GST-VCA and Arp2/3 (right graph). *B* and *C*, time to half-maximal polymerization was derived from bulk pyrene fluorescence curves for 1:3 and 1:1 ratios of R-actin to Ac-actin (2 μM total actin with 5% pyrene-labeled RMA). A representative example of three independent bulk fluorescence pyrene experiments is shown on the left. Statistical significance was tested by comparing the different actins using one-way ANOVA with a Tukey post-hoc test (N = 3). Ac-actin, acetylated actin; PFN, profilin-1; R-actin, arginylated β-actin.

While the data presented here begin to highlight a role of N-terminal actin modification in actin assembly dynamics, additional work will be needed to gain insight into the mechanisms underlying the differential effects of acetylation and arginylation of actin. In particular, it would be of interest to know whether N-terminal modification directly alters the electrostatic interactions between actin and actin-associated proteins or whether it influences the intrinsic interactions of actin monomers within the actin filament, which, by extension, indirectly influences the interaction with actin associated proteins.

Table 1
N-terminal modification of actin tunes actin filament assembly

Activity	Ac-actin	R-Actin	M-Actin
Nucleation	+++	+	+
Elongation	++	+	++
Elongation (mDia1)	++	+	+++
Arp2/3 nucleation	+++	+	+++
Severing	++	++	+++

Overview of the effects of actins with different N termini on the indicated actin-remodeling activities.

Experimental procedures

Protein expression and purification

N-terminally modified Ac-β-actin, R-β-actin, and M-β-actin

Constructs for expression of human Ac-β-actin, R-β-actin, and M-β-actin were generated and validated as described in Hatano *et al.* (21, 22). *Pichia pastoris* transformants for Ac-β-actin, R-β-actin, and M-β-actin, stored at −80 °C were revived on yeast extract-peptone-dextrose solid media plates at 30 °C. Cells were inoculated into 200 ml minimal glycerol medium liquid media composed of 1.34% yeast nitrogen base without amino acids (Sigma Y0626), 0.4 mg/l biotin, and 1% glycerol and cultured at 30 °C, 220 rpm. The culture medium was diluted to 6 L with fresh minimal glycerol media, and cells were further cultured at 30 °C, 220 rpm in six 2 L flasks until the absorbance at 600 nm (A_{600}) reached around 1.5. Cells were pelleted down by centrifugation (10,628*g* at 25 °C for 5 min, ThermoFisher Scientific #F9-6 × 1000 LEX rotor). The cells were washed once with sterilized water and resuspended into 6 L MM composed of 1.34% yeast nitrogen base without amino acids (Sigma Y0626), 0.4 mg/L biotin, and 0.5% methanol. Cells were cultured in twelve 2 l baffled flasks (500 ml for

each) at 30 °C, 220 rpm for 1.5 to 2 days, and 0.5 % methanol was fed every 24 h during the culture. Cells were pelleted down by centrifugation (10,628*g* at 25°C for 5 min, ThermoFisher Scientific #F9-6 × 1000 LEX rotor). Cells were washed once with water and suspended into 75 ml ice-cold water. The suspension was dripped into a liquid nitrogen bath and stored at −80 °C. Cell suspension (50 g) was loaded into a grinder tube (#6801, SPEX SamplePrep) precooled with liquid nitrogen. Cells were ground with freezer mill (#6870, SPEX SamplePrep) in a liquid nitrogen bath. Duration of the grinding was 1 min with 14 cycle per second (cps). The grinding procedure was repeated 30 times with 1 min intervals. Liquid nitrogen was refilled every 10th round of grinding. The resulting powder was kept on dry ice until the next step. The powder was thawed and resuspended in equal amounts of 2 × binding buffer [20 mM imidazole (pH 7.4), 20 mM Hepes (pH 7.4), 600 mM NaCl, 4 mM $MgCl_2$, 2 mM ATP (pH 7.0), 2× concentration of protease inhibitor cocktail (cOmplete, EDTA free #05056489001, Roche), 1 mM phenylmethylsulfonyl fluoride (PMSF), and 7 mM beta-mercaptoethanol]. The lysate was sonicated on ice (3 min, 5 s pulse, 10 s pause with 60% amplitude, QSONICA SONICATORS) until all aggregates were resolved. The lysate was centrifuged at 4 °C (3220*g* for 5 min, Eppendorf #A-4-81 rotor) to remove intact cells and debris. Insoluble fraction was removed by high speed centrifugation at 4 °C (25,658*g* for 30 min, ThermoFisher Scientific #A23-6-100 rotor). The supernatant was filtrated with 0.22 μm filter (Filtropur BT50 0.2, 500 ml Bottle Top Filter, #83.1823.101) and incubated with 6 ml Nickel resin (ThermoFisher Scientific #88222) at 4 °C for 1 h. The resin was pelleted down by centrifugation at 4 °C (1258*g* for 5 min, Eppendorf #A-4-81 rotor) and washed with ice-cold 50 ml binding buffer composed of 10 mM imidazole (pH 7.4), 10 mM Hepes (pH 7.4), 300 mM NaCl, 2 mM $MgCl_2$, 1 mM ATP (pH 7.0), and 7 mM beta-mercaptoethanol for four times. The resin was washed five times with G-buffer composed of 5 mM Hepes (pH 7.4), 0.2 mM $CaCl_2$, 0.01 w/v% NaN_3, 0.2 mM ATP (pH 7.0), and 0.5 mM dithiothreitol (DTT). The resin was suspended into ice-cold 40 ml G-buffer with 5 μg/ml TLCK-treated chymotrypsin (Sigma #C3142-25 MG) and incubated overnight at 4 °C. The chymotrypsin was inactivated by 1 mM PMSF, and the elution was collected into a tube. Actin retained on the resin was eluted with 12 ml G-buffer (without DTT for labeling), and all elution fractions were combined. The eluent with R-β-actin was divided to perform labeling of half of the protein. Each portion was concentrated with 30 kDa cut-off membrane (Sigma #Z677892-24EA) to 0.9 ml and 2.5 ml. Ac-β-actin, M-β-actin, and D-β-actin were not labeled, and hence, the eluent of each actin was concentrated to 0.9 ml. The 0.9 ml of each actin was polymerized by adding 100 μl of 10× MKE solution composed of 20 mM $MgCl_2$, 50 mM ethylene glycol tetraacetic acid (EGTA), and 1 M KCl for 1 h at room temperature and was kept unlabeled. The 2.5 ml of R-β-actin sample was desalted to remove DTT leftovers by using PD-10 (Prepacked Disposable PD-10 Columns, GE Healthcare #17085101) column pre-equilibrated with G-buffer without DTT. Then 100 mM KCl and 2 mM $MgCl_2$ were added into the desalted actin solution, and the sample was rotated in cold room for 1 h to induce actin polymerization. Next 3-fold excess of Alexa Fluor 647 C2 Maleimide (ThermoFisher Scientific #A20347) was mixed with the solution, and the mixture was incubated at room temperature for 1 h. The cysteine-maleimide reaction was quenched by addition of 10 mM DTT at 4 °C. The solution was centrifuged at ∼3220*g* for 5 min (Eppendorf #A-4-81 rotor) to pellet down precipitated dyes. The labeled and unlabeled polymerized actin samples were pelleted down by ultracentrifugation at room temperature (45,000 rpm for 1 h, Beckman TLA-55 rotor). The pellets were rinsed once with 1 ml G-buffer and re-suspended into ice cold 0.5 ml G-buffer. The actin was depolymerized by dialysis against 1 L G-buffer at 4 °C for 2 days. The dialysis buffer was exchanged every 12 h. The solutions with the depolymerized labeled and unlabeled actin were collected into 1.5 ml centrifuge tubes and stored on ice.

RMA, labeled RMA, and actin-regulatory proteins

Rabbit muscle actin (RMA), pyrene-labeled RMA, and Alexa Fluor 488-labeled RMA was purified as described in Graziano *et al.* (29). Plasmids pTYB11-mDia1(FH1-FH2) and pTYB11-HsPFN1 were kindly provided by Dr R. Dominguez (UPenn). pET15b-HsCof1 and pGAT2 GST-VCA (421–505) Hs N-WASP were obtained from Dr Bruce Goode (Brandeis University). All aforementioned proteins were expressed in Rosetta (DE3) *E. coli* by growing cells at 37 °C in TB medium to log phase, then inducing expression with 0.5 mM isopropyl β-d-1-thiogalactopyranoside (IPTG) at 18 °C for 16 h. Cells were harvested by centrifugation and stored at −80 °C until purification.

mDia1(FH1-FH2) and HsPFN1 were purified as described in Drazic *et al.* (11). Purification of HsCof1 occurred as described in Jansen *et al.* (29).

For purification of pGAT2 GST-VCA (421–505) HsN-WASP, the frozen pellet was resuspended in 3-fold volume of 1× PBS (137 mM NaCl, 2.7 mM KCl, 10 mM Na_2HPO_4, 1.8 mM KH_2PO_4), protease inhibitor mix, 1 mM PMSF, and 4 mM benzamidine. Next, the bacterial cells were lysed by three passes through a microfluidizer and cleared by centrifugation at 30,000*g* for 20 min. The cleared lysate was passed over glutathione sepharose 4B resin (GE Heathcare) by gravity, and the resin was washed with at least 10 column volumes of 1× PBS. Bound proteins were eluted by 1× PBS with 10 mM reduced glutathione (Sigma Aldrich). Fractions containing VCA-NWASP were concentrated and dialyzed to 20 mM Tris (pH 7.4), 150 mM NaCl, and 1 mM DTT, aliquoted, snap-frozen in liquid N_2, and stored at −80 °C until use. Protein concentration was determined spectrophotometrically by measuring the absorbance at 280 nm and using a calculated extinction coefficient of 5500 M^{-1} cm^{-1}.

Arp2/3 complex was purified from cryoground bovine brain (Pel-freez) using a modified protocol (30). Briefly, 200 g of frozen brain powder was resuspended in 400 ml of resuspension buffer (20 mM Tris (pH 8.0), 120 mM NaCl, 5 mM $MgCl_2$, 5 mM EGTA, 1 mM DTT) with protease inhibitor mix,

1 mM PMSF, and 4 mM benzamidine, and clarified by centrifugation at 12,000*g* for 30 min. The cleared supernatant was loaded onto Q–sepharose Fastflow resin (GE Healthcare) pre-equilibrated with resuspension buffer. The flow-through, containing Arp2/3 complex, was applied onto a VCA-HsNWASP affinity column equilibrated with resuspension buffer supplemented with 0.1 mM ATP. Bound Arp2/3 complex was eluted in 20 mM Tris (pH 8.0), 25 mM KCl, 400 mM $MgCl_2$, 1 mM EGTA, 1 mM DTT, 0.1 mM ATP, and dialyzed against 20 mM MES (pH 6.4), 20 mM KCl, 2 mM $MgCl_2$, 1 mM EGTA, and 0.1 mM ATP, before further purification on a Mono S column (GE Healthcare) using a 20 mM -1M KCl gradient. Peak fractions were combined and dialyzed against 20 mM Tris HCl (pH 7.5), 50 mM KCl, 2 mM MgCl2, 1 mM DTT, 10% glycerol, 1 mM DTT, 0.1 mM ATP, aliquoted, snap-frozen in liquid N_2, and stored at −80 °C until use. The concentration of the purified complex was determined spectrophotometrically using a theoretically calculated extinction coefficient of 234,080 M^{-1} cm^{-1}.

PFN binding

Differentially modified actin monomers (1 μM) were polymerized by addition of 50 mM KCl and 2 mM $MgCl_2$ for 1 h at room temperature in the presence of increasing concentrations (0–8 μM) of PFN. Filaments were collected by centrifugation at 90,000 rpm for 1 h at 25 °C. Actin in the supernatants and pellet fractions was visualized by UV-exposure of TGX stain-free gels and measured using densitometry to determine the percentage of actin in the pellet. Fraction of actin bound to PFN (*i.e.*, fraction of actin that was sequestered and thus does not polymerize) was calculated as 1 – [fraction of actin in pellet]. Fractions of bound actin plotted against [PFN] were used to obtain a binding curve and apparent K_d through nonlinear regression analysis. The average apparent K_d ± SD of three independent experiments is shown in the graph.

Pyrene fluorescence assays

Gel-filtered monomeric rabbit muscle actin (5–10% pyrene-labeled) was converted to Mg–ATP–actin immediately before use in each reaction and mixed with control buffer or the indicated concentrations of PFN-mDia1, GST-VCA, and Arp2/3 and 3 μl of 20× initiation mix (200 mM imidazole, pH 7.0, 1M KCl, 20 mM $MgCl_2$, and 20 mM EGTA) in 60 μl reactions. Actin polymerization was monitored over time at 365 nm excitation and 407 nm emission in a FS5 fluorometer (Edinburgh Instruments) at 25 °C. Time to half maximal polymerization (n = 3) was determined for each reaction. Statistical significance was analyzed using an unpaired Student's *t* test.

TIRFM

Prior to experiments, all actins were dialyzed overnight against G-buffer (3 mM Tris pH 7.5, 0.5 mM DTT, 0.2 mM ATP pH 7.0, and 0.1 mM $CaCl_2$). Next day, actins were cleared by high-speed centrifugation at 316,613*g* for 1 h at 4 °C in a TLA100 rotor (Beckman Coulter). Only the top 80% of the supernatant was collected to perform TIRFM. Labeling efficiency and concentration was determined for each actin after centrifugation using a DS-11+ spectrophotometer (Denovix). Labeling of Alexa-488-actin was calculated by measuring absorbance at 290 and 494 nm using the extinction coefficient of 72,000 M^{-1} cm^{-1}, and a Alexa488 correction factor of 0.138.

For all TIRFM experiments, coverslips were sonicated for 1 h in detergent, 20 min in 1 M KOH, 20 min in 1 M HCl, and 1 h in 100% ethanol. Clean coverslips were then rinsed with ddH_2O, dried extensively in an N_2-stream, and coated with 200 μl/slide of freshly prepared coating solution (80% ethanol pH 2.0, 2 mg/ml methoxy-(ethylene glycol)-silane, and 4 μg/ml biotin-poly(ethylene glycol-silane)). Coated coverslips were incubated overnight at 70 °C for 16 h, rinsed extensively with ddH_2O, dried in an N_2-stream, and attached to a flow chamber with double sided tape (2.5 cm × 2 mm × 120 μm) and 5 min epoxy resin. Each flow chamber was prepared immediately preceding each reaction as follows: 3 min incubation in 1% HBSA (1% BSA in 10 mM Imidazole pH 7.4, 50 mM KCl), 30 s incubation 4 mg/ml Streptavidin, washed with 1% HBSA, and finally equilibrated with 1× TIRF buffer (20 mM Imidazole pH 7.4, 100 mM KCl, 0.4 mM ATP pH 7.0, 2 mM MgCl2, 2 mM EGTA, 20 mM DTT, 30 mM glucose, 0.5% methylcellulose 4000 cP). To initiate reactions, modified actin monomers were rapidly diluted to 1 μM final concentration (containing 0.25–0.5% biotinylated RMA, and 10% Alexa488-RMA) in 1× TIRF buffer supplemented with 2 mg/ml catalase and 10 mg/ml glucose oxidase and transferred into a flow chamber. To measure nucleation, elongation, and branching, the actin-binding proteins of interest were included in the 1×TIRF buffer mix before addition of the actin monomers and transfer into the flow chamber. To measure severing/disassembly, actin monomers were polymerized at room temperature until filaments reached approximately 15 μm in length, then free monomers were washed out and Cof1 was flowed in. Time-lapse TIRF imaging was performed with a Ti2-LAPP inverted microscope equipped with through-the-objective TIRF illumination (Nikon), a LU-4N 4-laser unit (Nikon) and an iXon Ultra 888 EMCCD camera (Andor Technology). The pixel size corresponds to 0.217 μm.

TIRF analysis

TIRF data were analyzed using ImageJ software. To start, background fluorescence was subtracted using the background subtraction program and a rolling ball radius of 10 pixels. Filament nucleation rates were calculated by counting the number of filaments in a 130 μm × 130 μm box (5 squares per reaction) at 5 min after start of the reaction. For each reaction, dilution of actin monomers in the TIRFM buffer was taken as the start of the reaction. Filament elongation rates were determined by measuring the change in filament length over time (at least 60 s).

Arp2/3-mediated actin filament branching was measured by counting the total number of branches formed at specific time

points (4–14 min) after start of the reaction for equally large fields of view (FOVs) (150 × 150 micron). To exclude overlapping filaments, each branch was traced back to its first appearance, and only counted as a branch if it would grow off of another filament for at least 1 min. To account for differences in actin filament nucleation, the branching rate (# branches/min) was normalized to the total actin filament length (# branches/total actin filament length/min).

Cofilin-mediated filament severing was analyzed by counting the number if severing events observed during the next 600 s after flow-in of Cof1. To account for differences in the number and length of filaments between FOVs, severing was normalized to the initial length of the filament analyzed, *i.e.*, the length of the filament before flow-in of Cof1. Time to half-maximal severing for each FOV was determined from cumulative severing curves and used for statistical analysis. Best curve fit ($R^2 \geq 0.97$) was obtained using the equation for specific binding with Hill slope.

Statistical analysis

Statistical analysis and curve fitting was performed using Prism 9.3.1. The specific curve fitting algorithms used for each experiment are described in the TIRF analysis section. The distribution of nucleation, elongation, and branching rates are represented as bee swarms, overlaid with box-and whisker plots that show minimum, median, and maximum. Statistical significance between the distributions of the differently modified actins was analyzed by one-way ANOVA with a Tukey post-hoc test.

Data availability

Mass spec data confirming the purity of N-terminal modification of Ac-actin, R-actin, and M-actin were published in Hatano *et al.*, 2018 (https://doi.org/10.1242/jcs.213827) and 2020 (https://doi.org/10.1242/jcs.241406). Detailed data are available by request. Please contact M.K.Balasubramanian@warwick.ac.uk.

Supporting information—This article contains supporting information.

Author contributions—S. C., L. S., A. S. investigation; S. C. formal analysis; T. H. methodology; A. S. K., S. J., and M. K. B. conceptualization; M. K. B. resources; S. J. writing–review and editing.

Funding and additional information—The work in the laboratory of M. K. B. was supported by a Wellcome Trust Collaborative Award in Science (203276/Z/16/Z), a European Research Council Advanced Grant (ERC-2014-ADG No. 671083), and a collaborative BBSRC award to M. K. B. (BB/S003789/1). The work in the A. S. K laboratory was supported by NIH grants R35GM122505 and R01NS102435. The content is solely the responsibility of the authors and does not necessarily represent the official views of the National Institutes of Health.

Conflict of interest—The authors declare that they have no conflicts of interest with the contents of this article.

Abbreviations—The abbreviations used are: Ac-actin, acetylated actin; DTT, dithiothreitol; EGTA, ethylene glycol tetraacetic acid; M-actin, actin with an N-terminal methionine; PFN, profilin-1; PMSF, phenylmethylsulfonyl fluoride; R-actin, arginylated β-actin; RMA, rabbit muscle actin; TIRF, total internal reflection fluorescence; TIRFM, TIRF microscopy.

References

1. Blanchoin, L., Boujemaa-Paterski, R., Sykes, C., and Plastino, J. (2014) Actin dynamics, architecture, and mechanics in cell motility. *Physiol. Rev.* **94**, 235–263
2. Krause, M., and Gautreau, A. (2014) Steering cell migration: lamellipodium dynamics and the regulation of directional persistence. *Nat. Rev. Mol. Cell Biol.* **15**, 577–590
3. Kaksonen, M., and Roux, A. (2018) Mechanisms of clathrin-mediated endocytosis. *Nat. Rev. Mol. Cell Biol.* **19**, 313–326
4. Pollard, T. D. (2016) Actin and actin-binding proteins. *Cold Spring Harb Perspect. Biol.* **8**, a018226
5. A, M., Fung, T. S., Francomacaro, L. M., Huynh, T., Kotila, T., Svindrych, Z., *et al.* (2020) Regulation of INF2-mediated actin polymerization through site-specific lysine acetylation of actin itself. *Proc. Natl. Acad. Sci. U. S. A.* **117**, 439–447
6. Hung, R.-J., Pak, C. W., and Terman, J. R. (2011) Direct redox regulation of F-actin assembly and disassembly by mical. *Science* **334**, 1710–1713
7. Karakozova, M., Kozak, M., Wong, C. C. L., Bailey, A. O., Yates, J. R., Mogilner, A., *et al.* (2006) Arginylation of ß-actin regulates actin cytoskeleton and cell motility. *Science* **313**, 192–196
8. Terman, J. R., and Kashina, A. (2013) Post-translational modification and regulation of actin. *Curr. Opin. Cell Biol.* **25**, 30–38
9. Varland, S., Vandekerckhove, J., and Drazic, A. (2019) Actin post-translational modifications: the cinderella of cytoskeletal control. *Trends Biochem. Sci.* **44**, 502–516
10. Wilkinson, A. W., Diep, J., Dai, S., Liu, S., Ooi, Y. S., Song, D., *et al.* (2019) SETD3 is an actin histidine methyltransferase that prevents primary dystocia. *Nature* **565**, 372–376
11. Drazic, A., Aksnes, H., Marie, M., Boczkowska, M., Varland, S., Timmerman, E., *et al.* (2018) NAA80 is actin's N-terminal acetyltransferase and regulates cytoskeleton assembly and cell motility. *Proc. Natl. Acad. Sci. U. S. A.* **115**, 4399–4404
12. Pavlyk, I., Leu, N. A., Vedula, P., Kurosaka, S., and Kashina, A. (2018) Rapid and dynamic arginylation of the leading edge β-actin is required for cell migration. *Traffic* **19**, 263–272
13. Vedula, P., Kurosaka, S., MacTaggart, B., Ni, Q., Papoian, G., Jiang, Y., *et al.* (2021) Different translation dynamics of β- and γ-actin regulates cell migration. *eLife* **10**, e68712
14. Arnesen, T., Marmorstein, R., and Dominguez, R. (2018) Actin's N-terminal acetyltransferase uncovered. *Cytoskeleton* **75**, 318–322
15. Goris, M., Magin, R. S., Foyn, H., Myklebust, L. M., Varland, S., Ree, R., *et al.* (2018) Structural determinants and cellular environment define processed actin as the sole substrate of the N-terminal acetyltransferase NAA80. *Proc. Natl. Acad. Sci. U. S. A.* **115**, 4405–4410
16. Rebowski, G., Boczkowska, M., Drazic, A., Ree, R., Goris, M., Arnesen, T., *et al.* (2020) Mechanism of actin N-terminal acetylation. *Sci. Adv.* **6**, eaay8793
17. Wong, C. C. L., Xu, T., Rai, R., Bailey, A. O., Yates, J. R., Wolf, Y. I., *et al.* (2007) Global analysis of posttranslational protein arginylation. *PLoS Biol.* **5**, e258
18. Zhang, F., Saha, S., Shabalina, S. A., and Kashina, A. (2010) Differential arginylation of actin isoforms is regulated by coding sequence–dependent degradation. *Science* **329**, 1534–1537
19. Chen, L., and Kashina, A. (2019) Quantification of intracellular N-terminal β-actin arginylation. *Sci. Rep.* **9**, 16669
20. Drazic, A., Timmerman, E., Kajan, U., Marie, M., Varland, S., Impens, F., *et al.* (2022) The final maturation state of β-actin Involves N-terminal acetylation by NAA80, not N-terminal arginylation by ATE1. *J. Mol. Biol.* **434**, 167397

21. Hatano, T., Alioto, S., Roscioli, E., Palani, S., Clarke, S. T., Kamnev, A., *et al.* (2018) Rapid production of pure recombinant actin isoforms in Pichia pastoris. *J. Cell Sci.* **131**, jcs213827
22. Hatano, T., Sivashanmugam, L., Suchenko, A., Hussain, H., and Balasubramanian, M. K. (2020) Pick-ya actin - a method to purify actin isoforms with bespoke key post-translational modifications. *J. Cell Sci.* **133**, jcs241406
23. Pollard, T. D., and Cooper, J. A. (1984) Quantitative analysis of the effect of acanthamoeba profilin on actin filament nucleation and elongation. *Biochemistry* **23**, 6631–6641
24. Rotty, J. D., Wu, C., Haynes, E. M., Suarez, C., Winkelman, J. D., Johnson, H. E., *et al.* (2015) Profilin-1 serves as a gatekeeper for actin assembly by Arp2/3-dependent and -independent pathways. *Dev. Cell* **32**, 54–67
25. Suarez, C., Carroll, R. T., Burke, T. A., Christensen, J. R., Bestul, A. J., Sees, J. A., *et al.* (2015) Profilin regulates F-actin network homeostasis by favoring formin over Arp2/3 complex. *Dev. Cell* **32**, 43–53
26. Zimmermann, D., and Kovar, D. R. (2019) Feeling the force: formin's role in mechanotransduction. *Curr. Opin. Cell Biol.* **56**, 130–140
27. Saha, S., Mundia, M. M., Zhang, F., Demers, R. W., Korobova, F., Svitkina, T., *et al.* (2010) Arginylation regulates intracellular actin polymer level by modulating actin properties and binding of capping and severing proteins. *Mol. Biol. Cell* **21**, 1350–1361
28. A, M., Fung, T. S., Kettenbach, A. N., Chakrabarti, R., and Higgs, H. N. (2019) A complex containing lysine-acetylated actin inhibits the formin INF2. *Nat. Cell Biol.* **21**, 592–602
29. Jansen, S., Collins, A., Chin, S. M., Ydenberg, C. A., Gelles, J., and Goode, B. L. (2015) Single-molecule imaging of a three-component ordered actin disassembly mechanism. *Nat. Commun.* **6**, 7202
30. Boczkowska, M., Rebowski, G., Petoukhov, M. V., Hayes, D. B., Svergun, D. I., and Dominguez, R. (2008) X-ray scattering study of Activated Arp2/3 complex with bound actin-WCA. *Structure* **16**, 695–704